J Solid State Electrochem (2007) 11: 283–290
DOI 10.1007/s10008-006-0105-3

ORIGINAL PAPER

Yaomin Zhao · Ling Liu · Juan Xu · Jie Yang · Manming Yan · Zhiyu Jiang

High-performance supercapacitors of hydrous ruthenium oxide/mesoporous carbon composites

Received: 27 October 2005 / Revised: 18 January 2006 / Accepted: 24 January 2006 / Published online: 8 March 2006

Abstract The amorphous hydrous ruthenium oxide/mesoporous carbon composites (denoted as $RuO_2{\cdot}xH_2O$/MC), obtained by loading small amount of amorphous hydrous ruthenium oxide nanoparticles ranged from 0.9 to 5.4% by weight of Ru (denoted as $RuO_2{\cdot}xH_2O$) on mesoporous carbon (MC), were investigated for the first time and were used for supercapacitors. Electrochemical measurements showed that $RuO_2{\cdot}xH_2O$/MC composites not only have an enhanced specific capacitance but also retain the superior rate capability of MC. The $RuO_2{\cdot}xH_2O$/MC composite with Ru loading of 3.6 wt% exhibited an increase of the specific capacitance of approximately 57% (from 115 to 181 F/g) at the scan rate of 25 mV s^{-1} in 0.1 M H_2SO_4 aqueous electrolyte. The specific capacitance based on the mass of RuO_2 was estimated to be 1,527 F/g, by subtracting the contribution from MC in the composite. Cycle performance tests for $RuO_2{\cdot}xH_2O$/MC composite (3.6 wt% Ru) showed that approximately 2.8% loss of the total capacitance was observed after 1,000 cycles.

Keywords Hydrous ruthenium oxide · Mesoporous carbon · Supercapacitors · Composites

Introduction

Growing demands for power sources for transient high-power density have stimulated great interest in supercapacitors in recent years. Supercapacitors have been recognized as unique devices exhibiting much higher capacity and higher power characteristics in comparison with the electrolytic capacitor and most primary energy storage units, respectively. These advantages are good for a wide range of applications in the hybrid power sources for electrical vehicles, digital telecommunication systems, uninterruptible power supply (UPS) for computers, peak-power and backup-power sources, and the starting power source of fuel cells, etc [1, 2].

The mechanisms for the energy storage within supercapacitors can be divided into two categories: electric double-layer capacitors (EDLCs) and faradaic pseudocapacitors. In the former case, the energy is stored by charge separation formed at the interface between the electrode and the electrolyte. Carbon materials such as activated carbon (AC), mesoporous carbon (MC), carbon nanotubes (CNT), carbon aerogels, and so on, have been widely used as EDLC electrodes because of their high surface area. In the latter system, the electrodes of faradaic pseudocapacitors are formed from electroactive materials, which can store more energy by a fast faradaic reaction in the electrode at an appropriate potential. Ruthenium oxide is one of such kind of materials for supercapacitors, as the redox reactions of oxyruthenium species can be simply expressed as follows [2–5]:

$$RuO_a(OH)_b + \delta H^+ + \delta e^- = RuO_{a-\delta}(OH)_{b+\delta}$$

Thus, faradaic charges can be reversibly stored and delivered in $RuO_x{\cdot}nH_2O$ with mixed proton–electron conductivity [3, 4].

At present, activated carbons are widely used as EDLC electrode materials because of their low cost, wide variety of carbon precursors, and high surface area. They have wide pore size distributions extending over the whole micropore–mesopore range (0–50 nm) and their surface area are mainly contributed by micropores [6]. The small pore size of activated carbon has imposed some problems relating to the rate of molecule transport through the pores, and thus limited the application of the carbon as electrodes in electrochemical systems such as EDLCs to a certain degree, especially at high current densities. It is reported that only supermicropores (1–2 nm) and mainly mesopores (2–50 nm) are electrochemically accessible for ions.

Y. Zhao · L. Liu · J. Xu · J. Yang · M. Yan · Z. Jiang (✉)
Department of Chemistry, and Shanghai Key Laboratory of Molecular Catalysis and Innovative Materials,
Fudan University,
Shanghai 200433, People's Republic of China
e-mail: zyjiang@fudan.ac.cn
Tel.: +86-21-65642404
Fax: +86-21-65641740

Therefore, mesoporous carbon with high surface area and containing interconnected mesopores (>2 nm) are highly desirable for the EDLCs electrodes [6–8]. Recently, employing mesoporous silica templates for carbon preparation has been proven to be a promising technique through which carbons with uniform mesopores have been produced and used for supercapacitors [1, 6–12].

Ruthenium dioxide in both amorphous and crystalline forms has been widely recognized as an important electrode material in several fields, such as the chlor-alkali industry, water electrolysis, oxygen reduction, organic synthesis, waste effluents, electronics, electrocatalysis [13, 14], and supercapacitors [4]. In 1995, Zheng and Jow [15] and Zheng et al. [16] reported the high specific capacitance over 768 F/g of amorphous hydrous $RuO_2{\cdot}xH_2O$ for the first time. In 2004, the maximum specific capacitance of $RuO_2{\cdot}xH_2O$, 1580 F/g, was reported by Hu and Chen [3]. Recently, hydrous ruthenium oxides ($RuO_2{\cdot}xH_2O$), fabricated by solgel and modified solgel processes [2–5, 17], colloidal method [18], autocatalytic deposition [19], cyclic voltammetric deposition [20, 21], and the chemical oxidation method [22], have been shown to be one of the most promising materials for supercapacitors because of their high specific capacitance and highly electrochemical reversibility. However, how to improve the utilization of $RuO_2{\cdot}xH_2O$ is the major issue for its practical use due to its high cost. Therefore, the recent research has focused on improving the utilization of electroactive species to develop structures of RuO_2/carbon composite material to reduce the cost of material and increase its high rate performance. Many research groups loaded amorphous $RuO_2{\cdot}xH_2O$ on various activated carbons [3–5, 17–19, 23], CNTs [24–26], and carbon aerogels [27] for high energy density supercapacitors by various loading methods. However, there is little report on loading $RuO_2{\cdot}xH_2O$ on MC ($RuO_2{\cdot}xH_2O$/MC composites) for supercapacitors to our best knowledge.

The major interest of the present study is to prepare the $RuO_2{\cdot}xH_2O$/MC composites with different Ru loadings and investigate their capacitive performance by means of voltammetric and chronopotentiometric studies. In this work, mesoporous carbon was prepared from a template of hexagonal self-ordered mesoporous silica (SBA-15) using sucrose as the carbon source. A colloidal method was employed to prepare $RuO_2{\cdot}xH_2O$ nanoparticles. The $RuO_2{\cdot}xH_2O$/MC composites were prepared by liquid adsorption $RuO_2{\cdot}xH_2O$ nanoparticles in the form of colloid on MC followed by annealing at 200°C for 2 h in air. At the same time, their electrochemical properties were investigated in detail as compared with bare MC. Our studies indicated that the $RuO_2{\cdot}xH_2O$/MC composites with small amount of Ru (0.9 to 5.4 wt%) possess enhanced specific capacitance and superior rate capability just as expected.

Experimental

Synthesis of mesoporous carbon

Ordered mesoporous carbon was synthesized according to the synthesis procedure reported by Jun et al. [28] by using the ordered mesoporous molecular sieve SBA-15 as the template and sucrose as the carbon source.

Typical procedure for the synthesis of SBA-15 is as follows: 5 g of Pluronic P123 triblock polymer ($EO_{20}PO_{70}EO_{20}$, Mn=5,800, Aldrich) and 28 g of distilled water were added to 150 ml of 2 M HCl and stirred for 4 h at 313 K. After that, 10 g of $Si(OC_2H_5)_4$ (TEOS) was added to the above mixture, and stirred for 30 min. The mixture was aged at 313 K under moderate stirring for 24 h, and then crystallized at 368 K for 3 days. The solid product was filtered, washed with distilled water, and dried at room temperature. Finally, it was calcined at 873 K in air for 5 h to remove the template P123 and was used as the MC template without any further treatment.

The calcined SBA-15 was twice impregnated with aqueous solution of sucrose containing sulfuric acid. Firstly, 10 g of SBA-15 was added to a solution obtained by dissolving 12.5 g sucrose and 1.4 g of H_2SO_4 in 50 g of H_2O. The mixture was ultrasonically dispersed for 30 min and then was placed in a drying oven for 6 h at 373 K. Subsequently, the oven temperature was increased to 433 K and maintained there for 6 h. The sample turned dark brown during the treatment in the oven. Secondly, the silica sample, containing partially polymerized and carbonized sucrose was treated for the second time at 373 K and 433 K using the same drying oven after the addition of 12.5 g of sucrose, 1.4 g H_2SO_4 in 50 g H_2O. Again, the above mixture was ultrasonically dispersed for 30 min. The carbonization was completed by pyrolysis with heating to 1,173 K for 6 h under highly purified nitrogen.

The carbon–silica composite obtained after pyrolysis was washed with 40 wt% HF solution twice at room temperature for 10 h to remove the silica template. The template-free carbon product thus obtained was filtered, washed with distilled water, and dried at 393 K.

Preparation of $RuO_2{\cdot}xH_2O$ nanoparticles

The $RuO_2{\cdot}xH_2O$ nanoparticles were prepared by following the procedure reported by Chi-Chang Hu et al. [4]. The $RuCl_3{\cdot}xH_2O$ precursors were dissolved and agitated in a solution with equal volumes of water and methanol to form the organometallic species at room temperature for 1 h. A 2-M KOH solution was then dropped into the stirred solution until the pH reached 7.0, and this solution was stirred with a magnetic stirring bar for 30 min. Black ruthenium precipitates were clearly found after sedimentation, which could be efficiently obtained by means of a centrifugation. The product was washed with distilled water several times until the pH≈7, and the residual chlorides in the sediments were confirmed to be lower than 10^{-5} M by titration with 0.1 M $AgNO_3$ solution. These

cleaned precipitates were redissolved into an aqueous 0.1 M NH_3 solution and were stirred in a water bath at 40°C for 8 h to form a colloid solution of $RuO_2{\cdot}xH_2O$.

Preparation of $RuO_2{\cdot}xH_2O$/MC composites

The $RuO_2{\cdot}xH_2O$ nanoparticles were loaded on the MC by liquid adsorption method to form the $RuO_2{\cdot}xH_2O$/MC composites. The specific procedure is as follows: The required amount of $RuO_2{\cdot}xH_2O$, in the form of colloid solution, and MC were placed in a beaker. The mixture was dispersed with an ultrasonic wave for 30 min at first, then was annealed at 60°C to remove most of the solvent, finally followed by annealing process at 200°C for 2 h in air. The $RuO_2{\cdot}xH_2O$/MC composite used for subsequent tests was then obtained. The loading amount in this work ranged from 0.9% to 5.4% by weight of Ru.

Characterizations

The low-angle powder X-ray diffraction (XRD) patterns were recorded on a Rigaku D/max-rB diffractometer with Cu–Ká radiation, operated at 60 mA and 40 kV. The specific surface areas, the pore volumes, and mean pore diameters of the mesoporous materials were measured and calculated according to the Brunauer–Emmett–Teller (BET) method on a Micromeritics Tristar ASAP 2000 apparatus at 77 K. Scanning electron micrographs (SEM) were carried out on a Philips XL 30 apparatus. The samples were deposited on a sample holder with an adhesive carbon tape and sputtered with a thin film of gold. Transmission electron micrographs (TEM), high-resolution transmission electron micrographs (HR-TEM), and selected area electron diffraction (SAED) were obtained on a Joel JEM 2010 scan-transmission electron microscope. The samples were supported on carbon-coated copper grids for experiments. The ruthenium content was determined by inductively coupled Argon plasma (ICP, IRIS Intrepid, Thermo Elemental Company) after solubilization of the samples in hot condensed HCl solutions.

For electrochemical measurement, the samples were mixed and ground with 5 wt% poly(tetrafluoroethylene) powder as a binder. The material loading on every electrode was 3 mg. The mixture was spread and pressed on an Au plate current collector (0.56 cm^2). Cyclic voltammetric (CV) and chronopotentiometric (CP) measurements were performed on a CHI660 electrochemical workstation (CHI, USA) with a three-electrode configuration in 0.1 M H_2SO_4 aqueous electrolyte. An Ag/AgCl electrode was used as the reference, and a piece of platinum plate (1 cm^2) was employed as the counter electrode. The potential range of all the electrochemical measurements was −0.2 to 0.8 V vs Ag/AgCl. A Luggin capillary was used to minimize errors due to iR drop in the electrolytes. For CV measurements, the potential sweep rate ranged from 1 to 200 mV s^{-1}. For CP measurements, the current load ranged from 1.8 to 35.7 mA/cm^2.

Results and discussions

Pore structure analysis of the samples

Figure 1a shows low-angle XRD patterns for both MC and SBA-15 silica. The presence of three diffraction peaks indexed as 100,110, and 200 for MC proves that MC was replicated from SBA-15. At the same time, it can also be clearly found that the diffraction peaks shifted to higher angle for MC as compared to SBA-15 template due to the shrinkage of mesopores at high temperature during the carbonization process [28]. In addition, the diffraction peaks of 110 and 200 are not so clearly observed for MC as compared to SBA-15, which indicates the prepared MC showed more disordered structure as compared with SBA-15 during the replication and template-removing process.

BET method was also employed to analyze the pore structure of the samples. The surface areas were calculated from BET equation and mesopore size distributions were calculated by using Barrett–Joyner–Halanda (BJH) model from the desorption branch of the isotherms. The pore size distribution curves of the $RuO_2{\cdot}xH_2O$/MC composites compared with MC are presented in Fig. 1b, which shows that the mesoporous structure of MC was retained by $RuO_2{\cdot}xH_2O$/MC composites with different loadings. The presence of uniform mesopores is believed to favor the rate

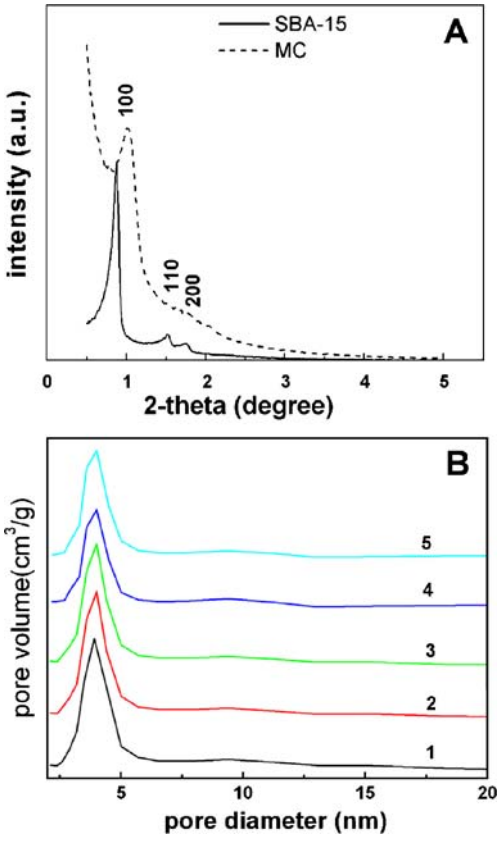

Fig. 1 **a** Low-angle XRD patterns for MC and SBA-15 silica template. **b** Pore size distributions of MC (1) and $RuO_2{\cdot}xH_2O$/MC composites with different Ru loadings of (2) 0.9, (3) 1.8, (4) 3.6, and (5) 5.4% by weight

capability of the mesoporous materials. The specific BET data used for characterization of the porous structure of the samples are listed in Table 1 for clarity. It can be clearly seen that the specific surface area and the pore volume of the composites decreased in a gradual way with the increase of Ru loading, and the BJH desorption average pore diameter remained almost unchanged. This result suggested that loading $RuO_2{\cdot}xH_2O$ nanoparticles on MC in our experiments does not decrease the specific surface area significantly and thus can give a better capacitive performance after the loading process due to the large pseudocapacitance based on $RuO_2{\cdot}xH_2O$ nanoparticles.

Morphological and crystalline characteristics

Figure 2 shows SEM and TEM (insets) images for MC (panel a, insets c and d) and $RuO_2{\cdot}xH_2O$/MC composite (panel b, insets e and f) annealed at 200°C for 2 h. From Fig. 2a, it can be seen that MC shows short and ruptured nanorods mostly due to the grinding process in the mortar before the measurements for the purpose of homogeneity. TEM images (c, d as insets in Fig. 2a) taken on the side of a primary carbon particle clearly shows that the carbon rods are aligned in parallel and thus the straight pores are developed inside the primary carbon particles. Figure 2b shows that the loaded RuO_2 particles were secondary aggregated particles composed of many small $RuO_2{\cdot}xH_2O$ clusters (≤10 nm). Meanwhile, it can also be seen from the insets (e, f) in Fig. 2b that these loaded particles were mostly distributed on the surface and at the pore opening of the MC nanorods. Therefore, after the loading process, the pore structure did not change and the BET surface of the composite did not decrease significantly, which was just desired for the capacitive properties.

Figure 3 shows the HR-TEM image of $RuO_2{\cdot}xH_2O$/MC composites annealed at 200°C for 2 h, and the typical SAED photograph presented as an inset in Fig. 3 confirmed the amorphous structure since there are no obvious diffraction rings [2]. The loading $RuO_2{\cdot}xH_2O$ nanoparticles with the mean diameter, about 1 nm, were observed from the HR-TEM image. This is because the capacitive behavior of hydrous ruthenium oxide is strongly structure-dependent and this highly dispersed structure is believed to be favorable for its electrochemical performance.

Table 1 BET data used for characterization of the porous structure of bare MC and $RuO_2{\cdot}xH_2O$/MC composites

Sample	BET surface area m^2/g	pore volume cm^3/g	BJH desorption average pore diameter nm
Bare MC	1,062	1.359	4.6
0.9 wt% Ru/MC	1,022	1.319	4.6
1.8 wt% Ru/MC	988	1.260	4.6
3.6 wt% Ru/MC	958	1.204	4.6
5.4 wt% Ru/MC	894	1.142	4.8

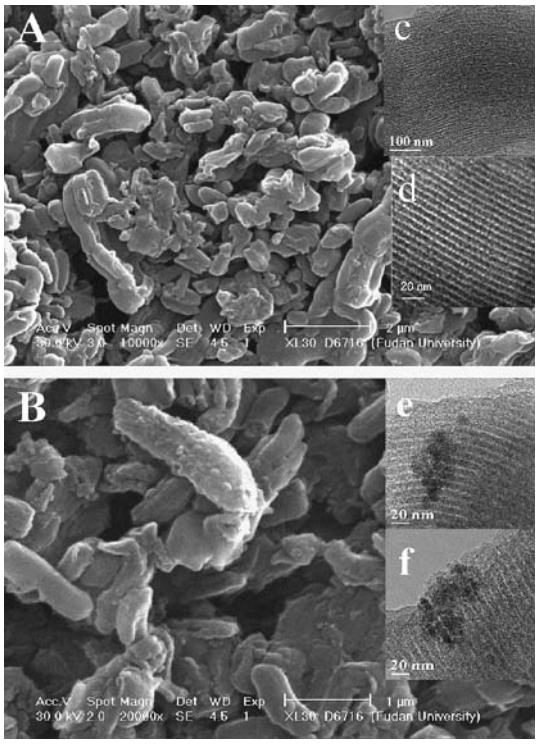

Fig. 2 **a** SEM and TEM (inset c and d) images of the mesoporous carbon (MC). **b** SEM and TEM (inset e and f) images of $RuO_2{\cdot}xH_2O$/MC composite (3.6 wt% Ru) annealed at 200°C for 2 h

Characteristics of supercapacitors

The cyclic voltammograms of bare MC and $RuO_2{\cdot}xH_2O$/MC composite (3.6 wt% Ru) annealed at 200°C for 2 h recorded at different potential sweep rates from 5 to 50 mV s^{-1} are presented in Fig. 4a and b, respectively. Figure 4c presents the CVs of $RuO_2{\cdot}xH_2O$/MC composites with different Ru loadings of (2) 0.9, (3) 1.8, (4) 3.6, (5) 5.4% by

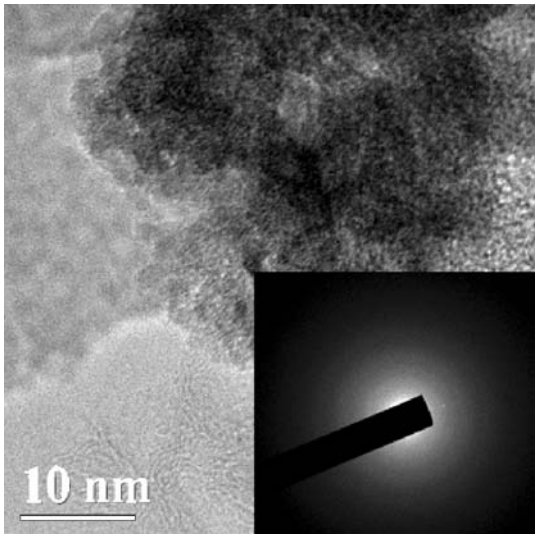

Fig. 3 HR-TEM photographs of $RuO_2{\cdot}xH_2O$/MC composite annealed at 200°C for 2 h (Inset is the typical SAED image)

weight compared with that of bare MC (1) at the scan rate of 5 mV s^{-1}.

Firstly, it can be seen from Fig. 4a and b that both bare MC and $RuO_2{\cdot}xH_2O$/MC composite (3.6 wt% Ru) showed ideal capacitive behavior at the scan rate from 5 to 50 mV s^{-1} within the potential range applied, which suggests that the $RuO_2{\cdot}xH_2O$/MC composite not only increased the energy density but also retained the superior capacitive properties of MC. Secondly, It can be seen from Fig. 4c that all the composites showed the same ideal capacitive behavior as bare MC and the specific capacitance increased proportionally with the increase of Ru loading.

It is interesting that a couple of highly reversible redox peaks present in the CVs for bare MC at about 0.2–0.4 V vs Ag/AgCl was also observed, which makes CV behavior of bare MC very similar to that of hydrous ruthenium oxide both in peak shape and peak position. The reversible redox process on carbon surface has been reported by a number of authors [7, 12, 29]. However, so obviously pronounced redox peaks for mesoporous carbon in 0.1 M H_2SO_4 electrolyte was reported for the first time to our best knowledge. This phenomenon can be explained as follows.

According to some related reports [29, 30], the redox process occurring on carbon surface includes two stages. First, surface oxygen functional groups were formed on the carbon surface determined by both the temperature of thermal treatment and the mechanical or electrochemical pretreatment of the sample. Second, the groups were reduced during the CV process and, thereafter, stable surface redox couples were formed at the end. It was reported that the formation of the functional groups starts with the oxidation of surface active sites, which are presumably defects of graphitic structural discontinuities in basal plane, not only at the edges of the layers, but in the interlayer spaces as well. In addition, carbon materials with less ordered structure, for example, thermally treated at lower temperature, are more readily activated especially in acidic than in neutral or alkaline media [29]. In this paper, mesoporous carbon was prepared at 900°C under highly purified nitrogen. This heating temperature only produced short-ranged ordered groups consisting of two or three randomly oriented imperfect parallel layers. What is more, a great amount of structural defects would be produced during the template-removing process in HF solution. The preparation process enables the prepared MC to have more pronounced redox signal in CV results in 0.1 M H_2SO_4 electrolyte than that for other carbon materials. Finally, it should be noted that these surface redox couples give a positive effect on the electrochemical properties of the carbon material, particularly enhanced specific capacitance. The pseudocapacitance capacitance from this redox reaction was estimated to contribute ca 16.94% of the total specific capacitance of MC determined by removing the surface oxygen groups by annealing MC in H_2 (3%)–Ar hybrid gas at 900°C for 1 h. Comparison of the first CV curves of MC before and after H_2(3%)–Ar hybrid gas annealing process is presented in Fig. 4d.

The capacitance data obtained from CVs in Fig. 4 were confirmed by chronopotentiometric studies. The capacitance of the electrode material can be evaluated from the

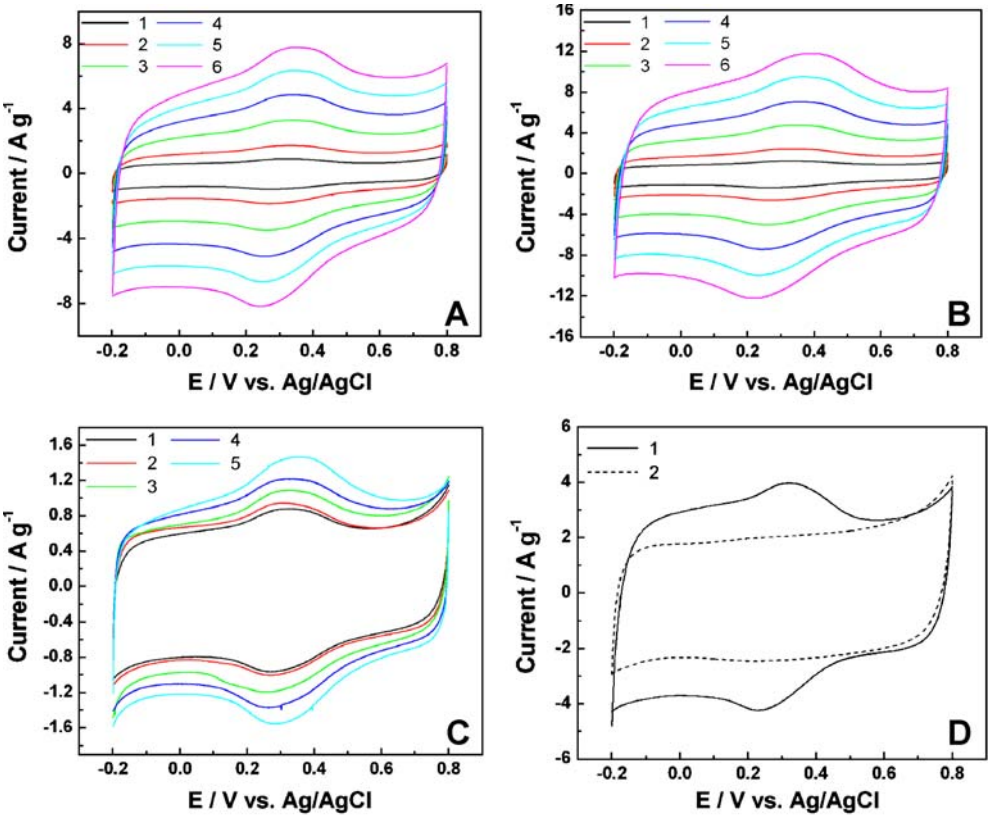

Fig. 4 Cyclic voltammograms of **a** bare MC, **b** $RuO_2{\cdot}xH_2O$/MC composite (3.6 wt% Ru) at the scan rate of (1) 5, (2) 10, (3) 20, (4) 30, (5) 40, (6) 50 mV s^{-1}. **c** Cyclic voltammograms of $RuO_2{\cdot}xH_2O$/MC composites with different Ru loadings of (1) 0, (2) 0.9, (3) 1.8, (4) 3.6, and (5) 5.4% by weight at the scan rate of 5 mV s^{-1} in 0.1 M H_2SO_4 aqueous electrolyte. **d** Comparison of the first cyclic voltammograms of MC before (1) and after (2) H_2 (3%)–Ar hybrid gas annealing process at 900°C for 1 h

slope of the discharge curves according to the formula below:

$$C = \frac{I \times \mathrm{d}t}{\mathrm{d}U} \quad (1)$$

When for simplicity, the charging curve is approximated by a linear function in the region dU, the medium integral capacitance values can be obtained as

$$\overline{C} = I \times \frac{\Delta t}{\Delta V \times m} \quad (\mathrm{F/g}) \quad (2)$$

$\overline{C}$ is the specific capacitance for a single electrode derived from chronopotentiometric curve, m is the weight of the single electrode, Δt is the charge or discharge time, and ΔV is the potential difference. In this study, m=3 mg, ΔV=1.0 V, and I=1.8~35.7 mA/cm^2. The electrode surface area is 0.56 cm^2.

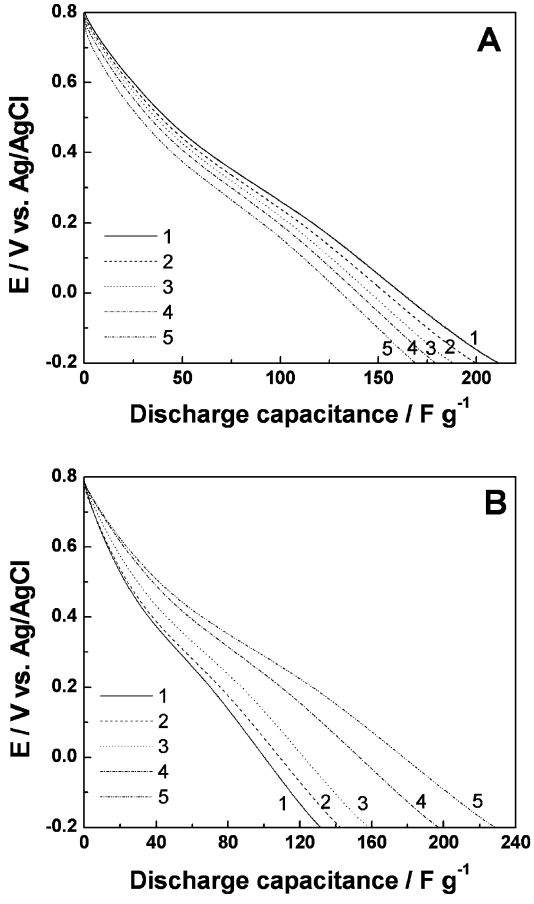

Fig. 5 **a** Discharge capacitance of $RuO_2{\cdot}xH_2O$/MC composite (3.6 wt% Ru) derived from chronopotentiograms at different current densities of (1) 1.8, (2) 3.6, (3) 8.9, (4) 17.9, and (5) 35.7 mA/cm^2. **b** Discharge capacitance derived from chronopotentiograms of bare MC (1) and $RuO_2{\cdot}xH_2O$–MC composites with different Ru loadings of (2) 0.9, (3) 1.8, (4) 3.6, and (5) 5.4% by weight at the current density of 8.9 mA/cm^2 in 0.1 M H_2SO_4 aqueous electrolyte

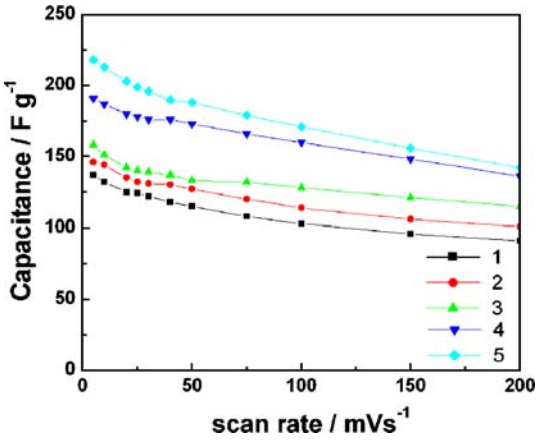

Fig. 6 Specific capacitance of (1) bare MC, $RuO_2{\cdot}xH_2O$/MC composites with Ru loading of (2) 0.9, (3) 1.8, (4) 3.6, and (5) 5.4 wt% as a function of scan rate in 0.1 M H_2SO_4 aqueous electrolyte

Figure 5a presents discharge capacitance estimated from the CPs of $RuO_2{\cdot}xH_2O$/MC composite (3.6 wt% Ru) annealed at 200°C for 2 h at different current densities of (1) 1.8, (2) 3.6, (3) 8.9, (4) 17.9, and (5) 35.7 mA/cm^2. As expected, when the current density was increased from 1.8 to 35.7 mA/cm^2, the specific capacitance decreased slightly from 205 to 169 F/g. This behavior occurred in the same manner in other composite electrodes, as well as bare MC (not shown here), which was characteristic of good rate capability. Figure 5b presents discharge capacitance derived from the CPs of $RuO_2{\cdot}xH_2O$/MC composites with different Ru loadings of (2) 0.9, (3) 1.8, (4) 3.6, and (5) 5.4% by weight compared with that of bare MC (1) at the current density of 8.9 mA/cm^2. The specific capacitance also increased from 130 F/g to 221 F/g, proportional with the increase of Ru loading from 0 to 5.4 wt%, which is in good agreement with CV results presented in Fig. 4.

The rate capabilities of all the $RuO_2{\cdot}xH_2O$/MC composites were investigated by CV measurements as compared with bare MC. The specific capacitance derived by CV measurements as a function of scan rate for bare MC (1),

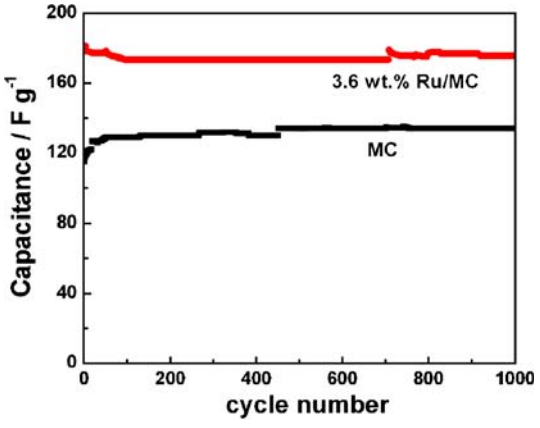

Fig. 7 Cycle performance of bare MC and the $RuO_2{\cdot}xH_2O$/MC composite (3.6 wt% Ru) during the first 1,000 cycles in 0.1 M H_2SO_4 aqueous electrolyte at a scan rate of 25 mV s^{-1}

$RuO_2{\cdot}xH_2O$/MC composites with different loadings of (2) 0.9, (3) 1.8, (4) 3.6, and (5) 5.4 by weight are presented in Fig. 6. The specific capacitance for bare MC and $RuO_2{\cdot}xH_2O$/MC composites was not so sensitive to the increasing scan rate, which clearly proves that the $RuO_2{\cdot}xH_2O$/MC composites not only had an increased specific capacitance but also retained the superior rate capability of bare MC. At the same time, it can be found that the rate capability of the composite showed the decline trend especially at the higher scan rate when the Ru loading amount increased to 5.4 wt%.

The cycle performance of bare MC and $RuO_2{\cdot}xH_2O$/MC composite with Ru loading of 3.6 wt% during the first 1,000 cycles at a scan rate of 25 mV s^{-1} was also tested by cyclic voltammetry. The specific capacitance as a function of cycle number for bare MC and $RuO_2{\cdot}xH_2O$/MC composite (3.6 wt% Ru) are shown in Fig. 7. It can be clearly found that bare MC and $RuO_2{\cdot}xH_2O$/MC composite showed different cycle behaviors. The specific difference was explained as follows. The specific capacitance of bare MC increased initially from 115 F/g, and 129 F/g was obtained after 100 cycles. An approximately constant capacitance of ca 134 F/g was found after 500 cycles. The phenomenon that the specific capacitance for MC increases during the initial scan process, which was called electrochemical activation, has been reported by other authors [7, 29, 30]. As for the $RuO_2{\cdot}xH_2O$/MC composite (3.6 wt% Ru), approximately 2.8% loss of capacitance (from 181 to 176 F/g) was observed after 1,000 cycles, and most of the capacity fade was observed initially. The obvious initial capacity fade for hydrous ruthenium oxide has been reported by other works [16, 18].

To calculate the specific capacitance of $RuO_2{\cdot}xH_2O$ from the total capacitance of $RuO_2{\cdot}xH_2O$/MC composites, it is necessary to estimate the amount of $RuO_2{\cdot}xH_2O$ in the electrode. By subtracting capacitance resulting from MC from the total capacitance, the specific capacitance on the basis of the mass of RuO_2 was estimated to be 1,527 F/g in case of 3.6 wt% at the scan rate of 25 mV s^{-1}. This capacitance data is very close to the reported maximum result, 1,580 F/g, which was determined at 1 mV s^{-1} on an AC-RuOx/RuOx/Au/SS electrode with 10 wt% solgel-derived $RuOx{\cdot}nH_2O$ also annealed in air at 200°C for 2 h [3]. The amorphous structure and the highly dispersed $RuOx{\cdot}nH_2O$ nanoparticles on the surface of MC in this paper and AC in the literature can account for the high specific capacitance of $RuOx{\cdot}nH_2O$.

Conclusions

Amorphous hydrous ruthenium oxide/mesoporous carbon powders ($RuO_2{\cdot}xH_2O$/MC) were prepared by liquid adsorption method. The mesoporous characteristics of mesoporous carbon and the high specific capacitance and highly electrochemical reversibility of $RuO_2{\cdot}xH_2O$ play a dominant role in the electrochemical properties of amorphous hydrous ruthenium oxide/mesoporous carbon ($RuO_2{\cdot}xH_2O$/MC) composites.

Electrochemical measurements showed that the $RuO_2{\cdot}xH_2O$/MC composites, prepared by loading small amount of $RuO_2{\cdot}xH_2O$ nanoparticles (ranging from 0.9 to 5.4 wt% Ru) on MC, not only have an enhanced specific capacitance (from 130 to 221 F/g at the current density of 8.9 mA/cm^2) but also retain the ideal capacitive performance such as highly reversibility, excellent rate capability, and good stability of MC. The $RuO_2{\cdot}xH_2O$/MC composite (3.6 wt% Ru) showed an increase of the specific capacitance by approximately 57% (from 115 to 181 F/g) at the scan rate of 25 mV s^{-1} in 0.1 M H_2SO_4 aqueous electrolyte within the potential range from −0.2 to 0.8 V vs Ag/AgCl. The specific capacitance of $RuO_2{\cdot}xH_2O$ was estimated to be 1,527 F/g, by subtracting the contribution from MC in the composite in case of 3.6 wt% Ru-loaded electrode at the scan rate of 25 mV s^{-1},which indicates the high utility of the active material $RuO_2{\cdot}xH_2O$. Cycle performance tests derived by CV measurements showed that 2.8% loss of total capacitance for the $RuO_2{\cdot}xH_2O$/MC composite (3.6 wt% Ru) was observed after 1,000 cycles. At the same time, the highly pronounced surface redox couples present for MC were discussed. The pseudocapacitance capacitance from this redox reaction was estimated to contribute ca 16.94% of the total specific capacitance of MC determined by removing the surface oxygen groups by annealing MC in H_2 (3%)–Ar hybrid gas at 900°C for 1 h.

Acknowledgement This work was supported by the National Science Foundation of China.

References

1. Fuertes AB, Lota G, Centeno TA, Frackowiak E (2005) Electrochim Acta 50:2799
2. Wang CC, Hu CC (2005) J Electrochem Soc 152(2):A370
3. Hu CC, Chen WC (2004) Electrochim Acta 49:3469
4. Hu CC, Chen WC, Chang KH (2004) J Electrochem Soc 151 (2):A281
5. Zhang J, Jiang D, Chen B, Zhu J, Jiang L, Fang H (2001) J Electrochem Soc 148(12):A1362
6. Fuertes AB, Pico F, Rojo JM (2004) J Power Sources 133:329
7. Liu HY, Wang KP, Teng H (2005) Carbon 43:559
8. Vix-Guterl C, Saadallah S, Jurewicz K, Frackowiak E, Reda M, Parmentier J, Patarin J, Beguin F (2004) Mater Sci Eng B108:148
9. Vix-Guter C, Frackowiak E, Jurewicz K, Friebe M, Parmentier J, Bėguin F (2005) Carbon 43:1293
10. Zhou H, Zhu S, Hibino M, Honma I (2003) J Power Sources 122:219
11. Jurewicz K, Vix-Guterl C, Frackowiak E, Saadallah S, Reda M, Parmentier J, Patarin J (2004) J Phys Chem Solids 65:287
12. Lee J, Kim J, Lee Y, Yoon S, Oh SM, Hyeon T (2004) Chem Mater 16(17):3323
13. Kumar AS, Pillai KC (2000) J Solid State Electrochem 4:408
14. Dharuman V, Pillai KC (2005) J Solid State Electrochem DOI 10.1007/s10008-005-0033-7
15. Zheng JP, Jow TR (1995) J Electrochem Soc 142:L6
16. Zheng JP, Cygan PJ, Jow TR (1995) J Electrochem Soc 142:2699
17. Chen WC, Hu CC, Wang CC, Min CK (2004) J Power Sources 125:292
18. Kim H, Popov BN (2002) J Power Sources 104:52

19. Ramani M, Haran BS, White RE, Popov BN (2001) J Electrochem Soc 148(4):A374
20. Hu CC, Huang YH (2001) Electrochim Acta 46:3431
21. Hu CC, Chang KH (2002) J Power Sources 112:401
22. Chang KH, Hu CC (2004) J Electrochem Soc 151(7):A958
23. Panic V, Vidakovic T, Gojkovic S, Dekanski A, Milonjic S, Nikolic B (2003) Electrochim Acta 48:3805
24. Arabale G, Wagh D, Kulkarni M, Mulla IS, Vernekar SP, Vijayamohanan K, Rao AM (2003) Chem Phys Lett 376:207
25. Park JH, Ko JM, Park OO (2003) J Electrochem Soc 150(7): A864
26. Kim JD, Kang BS, Noh TW, Yoon JG, Baik SI, Kim YW (2005) J Electrochem Soc 152(2):D23
27. Miller JM, Dunn B, Tran TD, Pekala RW (1997) J Electrochem Soc 144(12):L309
28. Jun S, Joo SH, Ryoo R, Kruk M, Jaroniec M, Liu Z, Ohsuna T, Terasaki O (2000) J Am Chem Soc 122:10712
29. Dekanski A, Stevanovic J, Stevanovic R, Nikolic BZ, Jovanovic VM (2001) Carbon 39:1195
30. Zuleta M, Bjo¨rnbom P, Lundblad A (2005) J Electrochem Soc 152(2):A270